




Electronic properties of hybrid organic/inorganic semiconductor pn-junctions

Moritz H Futscher^{1,3}, Thorsten Schultz¹, Johannes Frisch²,
Maryline Ralairisoa¹, Ezzeldin Metwalli³, Marco V Nardi¹,
Peter Müller-Buschbaum³ and Norbert Koch^{1,2}

¹ Institut für Physik & IRIS Adlershof, Humboldt-Universität zu Berlin, 12489 Berlin, Germany

² Helmholtz-Zentrum Berlin für Materialien und Energie GmbH-BESSY II, 12489 Berlin, Germany

³ Physik-Department, Lehrstuhl für Funktionelle Materialien, Technische Universität München, 85748 Garching, Germany

E-mail: norbert.koch@physik.hu-berlin.de

Received 24 September 2018, revised 19 November 2018

Accepted for publication 22 November 2018


Published 21 December 2018



Abstract

Hybrid inorganic/organic semiconductor heterojunctions are candidates to expand the scope of purely organic or inorganic junctions in electronic and optoelectronic devices. Comprehensive understanding of bulk and interface doping on the junction's electronic properties is therefore desirable. In this work, we elucidate the energy level alignment and its mechanisms at a prototypical hybrid pn-junction comprising ZnO (n-type) and p-doped N,N'-di(1-naphthyl)-N,N'-diphenyl-(1,1'-biphenyl)-4,4'-diamine (α -NPD) as semiconductors, using photoelectron spectroscopy. The level alignment can be quantitatively described by the interplay of contact-induced band and energy level bending in the inorganic and organic component away from the interface, and an interface dipole due to the push-back effect. By adjusting the dopant concentration in α -NPD, the position of the frontier energy levels of ZnO can be varied by over 0.5 eV and that of α -NPD by over 1 eV. The tunability of this pn-junction's energy levels evidences the substantial potential of the hybrid approach for enhancing device functionality.

Keywords: semiconductors, interfaces, electronic properties, photoelectron spectroscopy

 Supplementary material for this article is available [online](#)

(Some figures may appear in colour only in the online journal)

Introduction

Doping of semiconductors is a key method for optimizing the functionality of electronic and optoelectronic devices, allowing to tune the semiconductor's electrical and optical properties [1–4]. Compared to inorganic semiconductors, the fundamental mechanisms of doping organic semiconductors are not comprehensively understood [5, 6]. Particularly pn-junctions are of broad importance in electronic devices, such as diodes, transistors, and as charge generation/recombination contacts. The junction formation with intrinsic organic

semiconductors is quite well understood, and even organic pn-homojunctions have been realized [7, 8]. In contrast, inorganic/organic pn-junctions have not yet been realized, but they could open up new possibilities for material combinations and device functionality.

To provide insight into such a hybrid heterojunction, we investigate that of a ZnO single crystal, which has n-doped nature, and the exemplary organic hole-transport material N,N'-di(1-naphthyl)-N,N'-diphenyl-(1,1'-biphenyl)-4,4'-diamine (α -NPD), which we p-doped by intermixing with the strong molecular acceptor 2,2'-(perfluoronaphthalene-2,6-diylidene)dimalononitrile (F_6 TCNNQ). F_6 TCNNQ has a higher molar mass and thus lower volatility compared to the more commonly used 2,3,5,6-tetrafluoro-7,7,8,8-tetracyanoquinodimethane (F_4 TCNQ). This improves the thermal stability



Original content from this work may be used under the terms of the [Creative Commons Attribution 3.0 licence](#). Any further distribution of this work must maintain attribution to the author(s) and the title of the work, journal citation and DOI.

of dopants in the semiconductor matrix in devices and additionally prevents cross-contamination effects in multi-material sublimation chambers [5]. Furthermore, F₆TCNNQ has a slightly higher electron affinity compared to F₄TCNQ, implying more efficient host-to-dopant electron transfer [9].

Notably, molecular dopants, such as F₆TCNNQ, can also modify the electronic properties of inorganic semiconductor surfaces upon deposition. For ZnO and GaN it was shown that molecular acceptor deposition substantially increases the surface work function, accompanied by an upward surface band bending due to semiconductor-to-acceptor charge transfer [10, 11]. Furthermore, it is known that dopant molecules can diffuse through organic semiconductor matrices [6, 12–14], eventually resulting in preferential adsorption of dopants on the inorganic substrate when both compounds are co-deposited, as commonly done for fabricating organic doped layers. However, such diffusion can be substantially reduced or even absent for some amorphous matrix materials and densely packed molecular films [15, 16]. Consequently, it is of key importance in the context of interfaces with doped organic semiconductors to investigate to what extent dopant diffusion and/or preferential adsorption on the inorganic semiconductor impact the overall behavior of energy levels close to the interface. Therefore, in addition to discussing the electronic properties of α -NPD/ZnO based pn-junctions with varying doping levels of the organic layer, we contrast these with experiments on ZnO interfaces to the pristine organic compounds, as well as with a model of a pin-junction, i.e. an undoped α -NPD layer between ZnO and F₆TCNNQ. Indeed, we find that the acceptor alone substantially impacts the atomic and electronic structure of ZnO, and that diffusion of the acceptor through the α -NPD matrix is indeed negligible (on the timescale of our experiments). This allows us to quantify the electronic energy levels at this prototypical organic/inorganic pn-junction unambiguously, and thus providing first-time benchmark understanding of such junctions in general.

Experimental details

Zinc-terminated ZnO(0001) single crystals (purchased from CrysTec) were annealed in a GERO tube furnace under oxygen atmosphere at 1000 °C for 2h. The heating and the cooling rate were 33 °C and 3 °C per minute, respectively. After annealing the samples were either directly introduced into the vacuum chamber or stored in a glove box under nitrogen atmosphere to keep the exposure to air to a minimum. The ZnO surfaces feature large, atomically flat terraces and a sharp low-energy electron diffraction pattern (see the online supplementary information (SI), figure S1 (stacks.iop.org/JPhysCM/31/064002/mmedia)). F₆TCNNQ and α -NPD were purchased from Novaled and Sigma-Aldrich, respectively. Molecular thin films were prepared via sublimation from resistively heated quartz crucibles at residual gas pressure <10⁻⁶ mbar during evaporation. Doped films were prepared by co-sublimation of the two substances. The deposited materials' nominal mass thickness was monitored using a

quartz crystal microbalance, using a density of 1.35 g cm⁻³ for α -NPD and 1.65 g cm⁻³ for F₆TCNNQ.

Photoemission spectroscopy (PES) measurements were performed at HU Berlin and at the end station SurICat (beamline PM4) at synchrotron BESSY II in ultrahigh vacuum with base pressures of <10⁻⁹ mbar (HU) and <10⁻¹⁰ mbar (BESSY). Valence PES measurements were conducted using a differentially pumped Specs UVS 20-A He gas discharge lamp with a photon energy of 21.2 eV and a Specs EA 125 hemispherical electron energy analyzer with 5 eV pass energy (HU), as well as a photon energy of 40 eV and a Scienta SES 100 hemispherical electron energy analyzer with 20 eV pass energy (BESSY). The secondary electron cut-off (SECO) was measured at 2 eV pass energy applying a constant bias of -10 V to the sample to clear the analyzer work function. The contributions of the HeI _{β} and the HeI _{γ} satellites were subtracted from all shown UPS data measured at HU Berlin. Core level spectra were measured using Al K α radiation of an Omicron DAR-400 twin-anode x-ray source with 1486.6 eV at 20 eV pass energy (HU), and with photon energies of 1000 eV, 630 eV, and 500 eV at 50 eV pass energy for measuring the Zn2p, the O1s, and the N1s core level regions, respectively (BESSY). A clean polycrystalline gold substrate was used to determine the Fermi level position and the Au4f_{7/2} core level peak, set to 84 eV binding energy. XPS peak positions were determined by fitting the data with a Shirley background and Gaussian/Lorentzian (70:30) line shapes. The intersection of two straight lines fitted to the slope of the spectra and its background was used to determine the work function from the SECO and the low energy onset of the valence region. The energy resolution is 0.2 eV, including instrumental broadening and sample inhomogeneities.

Results and discussion

We start by investigating the electronic properties of interfaces formed between the individual organic compounds and ZnO, as well as an α -NPD interlayer between ZnO and the acceptor, for obtaining the key reference information that is required to ultimately understand the pn-junction itself, as outlined in the introduction. The changes of key parameters that characterize these interfaces, i.e. work function (Φ), substrate core level binding energies, and organic frontier energy level position, are summarized in figure 1 as function of overlayer thickness (corresponding PES spectra are shown in figures S2–S4 of the SI). Upon deposition of only 0.3 nm α -NPD onto ZnO, Φ decreases by 0.40 eV and stays constant for higher coverage (see figure 1(a)). In accordance with reported Φ changes upon α -NPD deposition on other metal oxides [17], we assign the Φ decrease observed in our case to the push-back effect, i.e. the electron density of ZnO that was spilling out into the vacuum for the bare surface is pushed back by surface-adsorbed α -NPD molecules. Since the core level positions of ZnO remain unchanged upon α -NPD deposition, no change occurs to the downward surface band bending that persist for the bare Zn-terminated ZnO surface [10, 11]. Consequently,

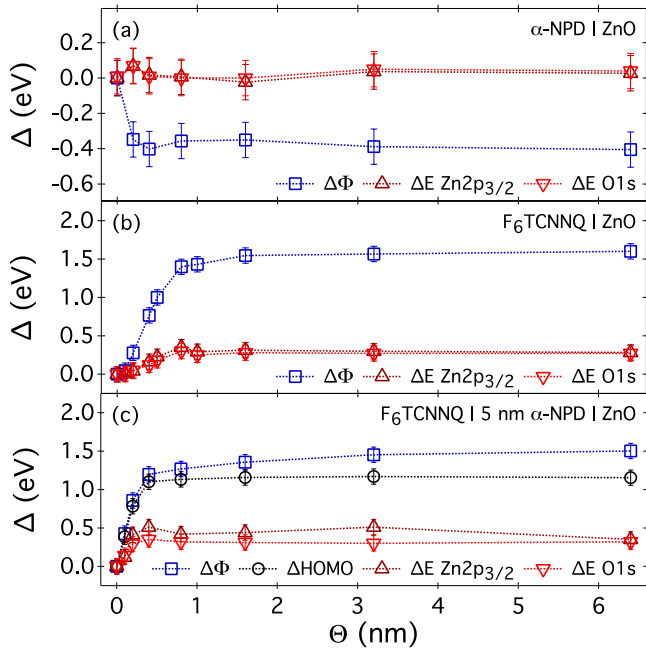


Figure 1. Relative changes of the work function (Φ) and core level positions of $Zn2p_{3/2}$ and $O1s$ as a function of nominal mass thickness (Θ) of (a) α -NPD on $ZnO(0001)$, (b) F_6TCNNQ on $ZnO(0001)$, and (c) F_6TCNNQ on 5 nm α -NPD on $ZnO(0001)$ (for corresponding PES spectra see figures S2–S4 in the SI).

the energy level alignment at the interface between α -NPD and ZnO is physisorptive and can be described by ‘push-back corrected vacuum level alignment’. The low binding energy onset of photoemission from the level associated with the highest occupied molecular orbital (HOMO) of α -NPD is 1.6 eV below the Fermi level (E_F) for multilayer coverage, and with a Φ value of 3.7 eV the ionization energy is 5.3 eV, in accordance with typical values reported for α -NPD [17–20].

The deposition of F_6TCNNQ on ZnO leads to a significant increase of Φ by up to 1.60 eV, due to electron transfer from ZnO to the molecular acceptor (see figure 1(b)) [11]. In accordance with observed Φ changes for similar molecular acceptors deposited on metals and on ZnO [10, 21], the saturation of Φ is assigned to the completion of a F_6TCNNQ monolayer, provided that multilayers do not further influence the work function, which has not yet been reported for such material systems. Since the nominal coverage (θ) of monolayer completion is larger than 1 nm, we suggest that island growth sets in before the monolayer closes. The Φ increase is accompanied by a shift of the $Zn2p_{3/2}$ and $O1s$ core level peaks by 0.30 eV to lower binding energy. The relative changes in the peak positions of the $Zn2p_{3/2}$ and $O1s$ core level peaks are shown in figure 1. Core level shifts of a semiconductor substrate upon deposition of molecular acceptors result in changes of the surface band bending. Consequently, the total work Φ upon adsorption of the acceptor on ZnO can be described by a change of surface band bending at the ZnO surface by 0.30 eV and a localized interface dipole of 1.30 eV due to the electron transfer to the acceptor, as explained in detail in [11]. In that same work it was shown that vacuum prepared ZnO surfaces exhibit a change in surface band-bending of up to 1.0 eV upon deposition of F_6TCNNQ and suggested that surface states of

ZnO significantly reduce band bending contributions to the Φ change. In comparison with our findings, we can conclude that ZnO surfaces that have been prepared *ex situ* by thermal annealing in oxygen atmosphere feature a higher surface state density than vacuum prepared ZnO surfaces. Furthermore, since the shifts saturate at the same coverage as the change of Φ , F_6TCNNQ monolayer completion at the corresponding coverage is substantiated.

Figure 1(c) shows the evolution of the key electronic parameters of incrementally deposited F_6TCNNQ onto ZnO pre-covered with a α -NPD interlayer with a nominal mass thickness of 5 nm. The zero shift values in figure 1(c) correspond to the work function, core level positions, and HOMO onset position for the pristine α -NPD interlayer on ZnO . Note that the absolute Φ value is 3.7 eV (due to the push back effect, *vide supra*), while Φ of bare ZnO is typically 4.1 eV in our experiments. The total change of Φ as well as the change of the surface band bending are the same, within the experimental error of less than 50 meV, for both F_6TCNNQ deposited directly on ZnO and with the α -NPD interlayer. However, due to the wider distance between F_6TCNNQ and the ZnO surface when the α -NPD interlayer is present (assuming no inter-diffusion of the organic compounds occurs), fewer molecules have to be negatively charged (compared to no interlayer) in order to achieve the same magnitude of the dipole [22]. Therefore, the saturation of the change in work function can be reached at a lower nominal thickness for F_6TCNNQ deposited on ZnO with α -NPD interlayer compared to F_6TCNNQ deposited directly on ZnO . We note that the difference in saturation coverage may also occur due to a difference in growth morphology between F_6TCNNQ deposited on ZnO with and without an α -NPD interlayer. Furthermore, the deposition of F_6TCNNQ on the α -NPD interlayer leads to a shift of the HOMO onset towards E_F by a notable amount (up to 1.15 eV). The HOMO onset position saturates at 0.55 eV below E_F (see SI figure S4).

The observations made for the α -NPD interlayer could have different underlying phenomena, which we discuss and evaluate in the following. If F_6TCNNQ were not able to p-dope α -NPD, then either long-range electron transfer from ZnO to the acceptor through the interlayer could take place, or F_6TCNNQ could diffuse through the interlayer and accumulate at the ZnO surface. However, since F_6TCNNQ is a stronger dopant than F_4TCNQ [15, 19, 23] and the fact that we observe distinct sub-band gap absorption features in optical spectroscopy (see figure S5 of the SI) for F_6TCNNQ -doped α -NPD films, which are representative of the acceptor anion species [24], we have evidence that F_6TCNNQ indeed p-dopes α -NPD.

Yet, possible dopant diffusion towards ZnO remains an important issue for pn-junction formation, as accumulation of dopants at ZnO (when dopant and semiconductor molecules are co-deposited) would modify the effective doping level close to the interface. A first indication that pronounced dopant diffusion is not present here is the fact that the saturation of all energy level shifts in the experiment with the α -NPD interlayer occurs at lower nominal F_6TCNNQ coverage than without interlayer (see figure 1), where actually

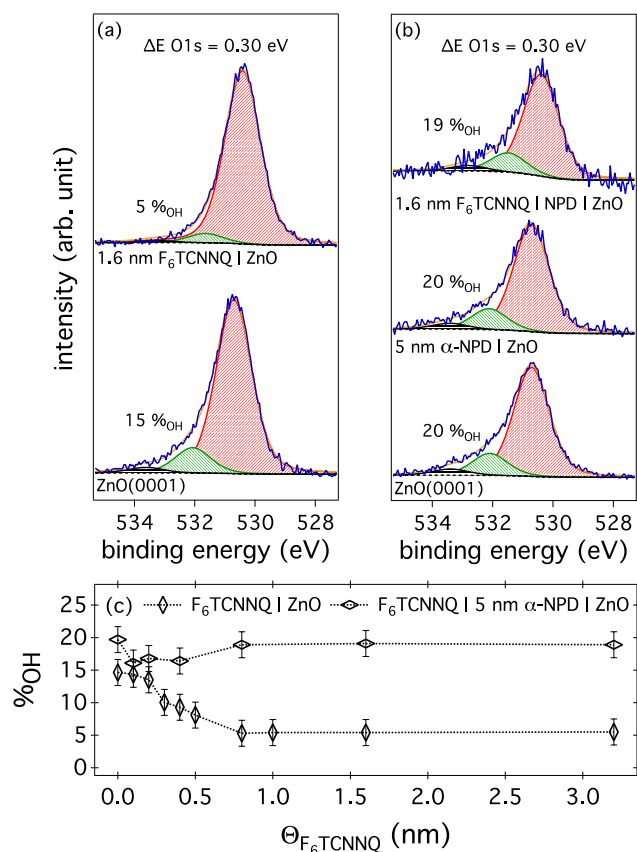


Figure 2. O1s core level spectra of 1.6 nm F₆TCNNQ deposited on (a) ZnO(0001) and (b) 5 nm α-NPD on ZnO(0001). (c) Ratio between the OH surface species and the bulk oxygen component (%OH) as a function of nominal mass thickness of F₆TCNNQ (Θ_{F₆TCNNQ}) on ZnO(0001) with and without α-NPD interlayer.

more molecules at a given coverage should reach ZnO. Clear evidence for the absence of notable F₆TCNNQ diffusion through a α-NPD matrix, however, comes from O1s core level spectra before and after F₆TCNNQ deposition on ZnO, with and without α-NPD interlayer (see figure 2). Based on theoretical modeling at the density functional level [25], the peaks observed in the O1s core level spectra of the ZnO(0001) polar surface are assigned to O²⁻ ions of the bulk ZnO lattice (red), surface OH groups (green), and OH groups filling oxygen vacancy sites (black). From XPS measurements with different photon energies, and thus different surface sensitivity, it becomes evident that both OH group types are surface species (see figure S6 of the SI). Note that the relative abundance of surface OH groups varies for different samples, as details of the surface morphology and storage history vary as well. After depositing F₆TCNNQ on ZnO we observe that the two OH surface species are considerably reduced with respect to the O1s core level of the bulk (see figure 2(a)). This indicates that F₆TCNNQ chemisorbs on ZnO involving a release of surface OH. Deposition of α-NPD has no effect on the OH surface loading (see figure 2(b)). From scanning force microscopy (SFM) measurements (see figure S7 of the SI) we conclude that the amorphous α-NPD layer with a nominal mass thickness of 5 nm covers the surface of ZnO completely.

Consequently, in the absence of diffusion, the interlayer of α-NPD could avoid direct contact between F₆TCNNQ and ZnO. Note that the reduction in OH surface groups may also be the reason for the observed difference in saturation coverage when depositing F₆TCNNQ on ZnO with and without an α-NPD interlayer (see figure 1). The evolution of the ratio between the surface OH species and the bulk oxygen versus the nominal F₆TCNNQ thickness with and without α-NPD interlayer is shown in figure 2(c). The constant ratio of the two oxygen types when depositing F₆TCNNQ on the α-NPD interlayer evidences that F₆TCNNQ does not diffuse notably through the α-NPD matrix (on the timescale of our experiment, i.e. several hours).

All above results enable the detailed and reliable characterization of the organic/inorganic pn-junctions, as described in the following in detail for α-NPD p-doped with 2 vol% F₆TCNNQ, and briefly summarized for higher dopant concentrations subsequently. Deposition of 0.1 nm of the p-doped α-NPD on ZnO results in a Φ reduction by 0.25 eV (see figure 3(a)), due to the push-back effect discussed for undoped α-NPD above. Further increasing the p-doped organic layer thickness leads to a continuous Φ increase, which saturates for coverages higher than ca. θ = 12.8 nm at a value of 4.85 eV. The initial Φ reduction due to the push-back effect is smaller than that for pristine α-NPD, as the effect induced by F₆TCNNQ, i.e. p-doping of α-NPD and thus shifting the Fermi level towards the HOMO level of the organic semiconductor, counteracts the push-back. On general grounds, we would argue that also for the p-doped α-NPD layer the actual push-back effect is around 0.40 eV, but not observed in the experiment as the upward energy level bending dominates (see also below for valence and core levels). Here we note that in contrast to covalent semiconductors, like ZnO, we do not use the term ‘band bending’ for the phenomenon in the molecular layer, as these amorphous materials do not exhibit bands but rather localized molecular levels; therefore, we use the term ‘energy level bending’. The increase in Φ for higher p-doped layer thickness is accompanied by a steady shift of the molecule derived frontier valence levels (seen already from 0.1 nm coverage onwards, see figure 3(b)), by a total amount of 0.85 eV. The HOMO level onset is constant beyond θ = 12.8 nm (as also observed for Φ), placed 0.50 eV below the Fermi level, resulting in a 0.95 eV reduction of its binding energy compared to pristine α-NPD on ZnO, as expected for p-type doping. The ionization energy of the 2 vol% doped α-NPD layer does not deviate notably from that of pristine α-NPD.

Observing the core level peak shifts allows differentiating between effects due to interfacial dipoles (e.g. the push-back and dopant-induced Φ changes) and actual doping-induced energy level bending. Upon increasing the coverage of p-doped α-NPD, the peak positions of N1s (figure 3(d)) shift to lower binding energies by 0.85 eV, attributed to energy level bending in the organic layer. Notably, the amount of this shift is identical to that observed for the valence features (figure 3(b)), supporting the notion of a purely electrostatic origin. We thus conclude on the formation of a space-charge region within the p-doped organic layer with upward energy level

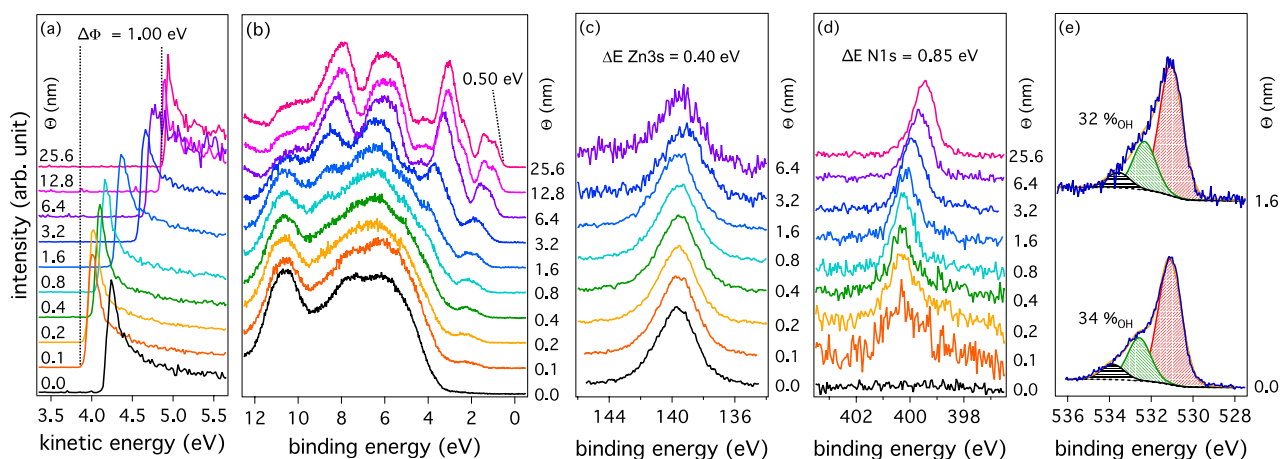


Figure 3. PES spectra of incrementally deposited α -NPD p-doped with 2 vol% F_6TCNNQ on ZnO. (a) Secondary electron cutoffs and (b) valance levels, obtained with 40 eV photon energy. Core level spectra of (c) Zn3s, (d) N1s, (e) and O1s, obtained using photon energies of 1000 eV, 500 eV, and 630 eV, respectively.

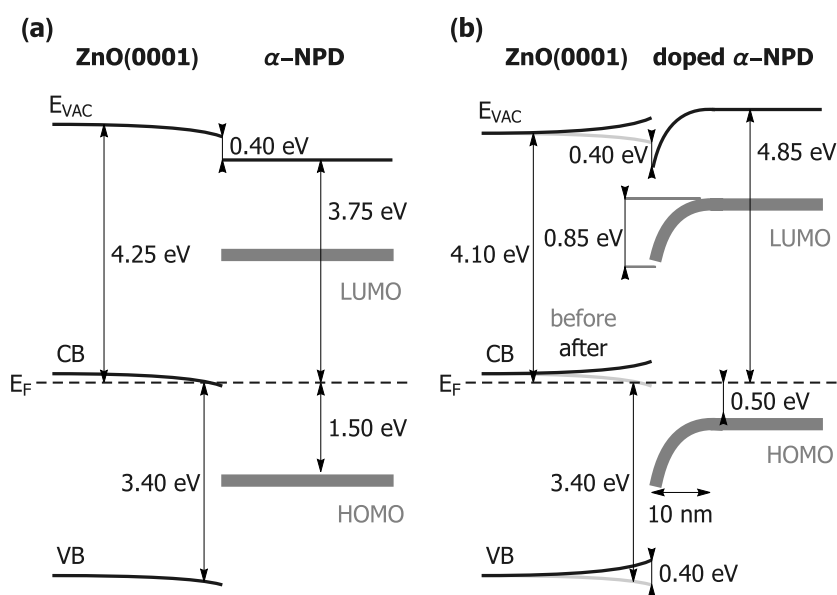


Figure 4. Schematic energy level diagrams at the hybrid interface between (a) α -NPD and ZnO(0001) and (b) α -NPD p-doped with 2 vol% F_6TCNNQ and ZnO(0001). Gray shaded energy bands indicate the energy levels of ZnO(0001) before molecular adsorption.

bending away from the interface. To minimize the error when considering the film thickness, so far given as nominal thickness θ from microbalance measurements during deposition, we assessed this value by mechanically scratching the sample and measuring the scratch height with SFM; the film thickness for $\theta = 25.6$ nm was found to be (19 ± 3) nm. Complete energy level bending is thus assumed to be reached at a film thickness of (10 ± 2) nm, corresponding to the thickness of the accumulation layer in the organic thin film. In contrast to the N1s core level, which is representative of the organic layer, the Zn3s (figure 3(c)) core level of ZnO gradually shifts to lower binding energy by up to 0.40 eV. This is assigned to a change of surface band bending within ZnO, due to electron transfer from ZnO to some of the molecular dopants within the p-doped α -NPD. Importantly, the amount of OH surface species is barely reduced (from 34% to 32%) upon p-doped α -NPD deposition (figure 3(e)), evidencing that the number of dopants directly adsorbing on ZnO is virtually negligible

(compare to figure 2 and its discussion above). Consequently, diffusion of F_6TCNNQ through the amorphous α -NPD matrix can indeed be neglected on the timescale of the experiment, as already concluded from the experiment with the 5 nm α -NPD interlayer above. The experimentally observed total work function change (starting from bare ZnO, i.e. +0.75 eV) observed upon p-doped α -NPD deposition on ZnO can be satisfactorily explained as the sum of the change in surface band bending in the inorganic substrate ($\Delta E \text{ Zn3s} = +0.4$ eV), the energy level bending in the organic film ($\Delta E \text{ N1s} = +0.85$ eV), and the estimated total contribution of the push-back effect ($E_{PB} = -0.4$ eV). The corresponding schematic energy level diagrams shown in figure 4 highlight the fundamental differences between the electronic properties of the hybrid organic/inorganic semiconductor heterojunction of in-type (intrinsic α -NPD and n-type ZnO) and pn-type (p-type α -NPD and n-type ZnO), whereas the pn-junction features the band (energy level) bending behavior in both layers away from the

interface, as known from conventional inorganic pn-junctions. We note that there is no noticeable diffusion of oxygen from the ZnO substrate on the timescale of the experiment, as the O1s and the Zn2p core levels are equally attenuated and no oxygen can be detected after a thick film of α -NPD p-doped with 2 vol% F₆TCNNQ has been deposited on ZnO (see SI figure S10).

To provide an estimate of the doping efficiency of F₆TCNNQ for α -NPD, which is defined as the ratio of mobile charge carriers to the number of dopants present, established semiconductor theory may be used [7, 19, 26]. Assuming that the dopant density in α -NPD is much higher than the dopant density in ZnO, the width of the accumulation layer can be approximated by [27]

$$w \approx \sqrt{\frac{2 \varepsilon \varepsilon_0 V_b}{e N_A}}$$

where V_b is the energy level bending magnitude in α -NPD and N_A is the dopant density calculated as

$$N_A = \delta \frac{L \rho_{\text{NPD}}}{M_{\text{NPD}}}$$

where δ is the nominal doping ratio (obtained from the vol% values used above), L the Avogadro constant, and ρ_{NPD} and M_{NPD} are the density and the molar mass of α -NPD, respectively. The dielectric constant is assumed to be $\varepsilon = 3$, which is a value often used for organic semiconductors. Using the measured energy level bending of 0.85 eV and the accumulation layer width of (10 ± 2) nm, we derive a doping efficiency of $(5 \pm 3)\%$, corresponding to a density of mobile holes of $(3 \pm 2) \times 10^{18} \text{ cm}^{-3}$ within the p-doped α -NPD, compared to a dopant density N_A of $5 \times 10^{19} \text{ cm}^{-3}$. This shows that only a small fraction of the dopants can introduce mobile holes that contribute to conduction. Similar low doping efficiencies, of only a few percent, have indeed been reported earlier for p-type doping of organic semiconductors [28–30]. The low doping efficiency can be attributed to the strong Coulomb interaction in these materials [31–33], which means that positive charges on a semiconductor molecule remain strongly bound to the dopant anions, and therefore do not enhance electrical conductivity. However, also local structural details and trap states, originating from chemical impurities and/or structural disorder were found to play an important role [34, 35].

Finally, we attend to a wider range of dopant concentrations. Figure 5 shows the evolution of valence and core levels, as well as the work function of the intrinsic and differently p-doped α -NPD films on ZnO(0001), all with a nominal mass thickness θ of 5 nm. Note that this film thickness does not yet correspond to the thick-film limit, i.e. the shown values are still within the accumulation region, particularly for low doping levels. With increased doping concentration N_{dop} (given in vol%) Φ increases by up to 1.45 eV and the HOMO level of α -NPD shifts by 1.20 eV towards the Fermi level, both compared to an undoped α -NPD film on ZnO. The changes of Φ and HOMO level saturate at N_{dop} between 10 vol% and 20 vol%, with the lowest value for the HOMO onset at 0.40 eV

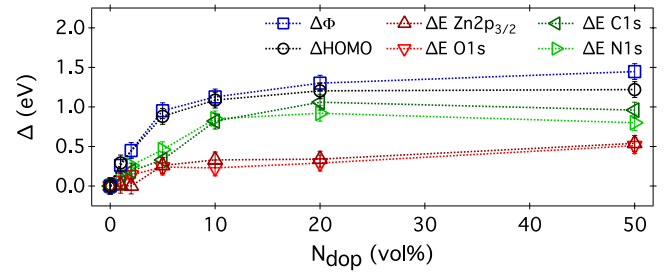


Figure 5. Dependence of the work function (Φ), the HOMO onset (Δ HOMO) and core level position of Zn2p_{3/2}, O1s, C1s, and N1s as a function of F₆TCNNQ doping concentration (N_{dop}) in α -NPD films on ZnO(0001). All molecular films have a nominal thickness of 5 nm (see SI figure S9 for corresponding PES spectra).

below the Fermi level. The ionization energy at low N_{dop} corresponds to the one of pristine α -NPD. In accordance with F₄TCNNQ-doped molecular films [15], the ionization energy at high N_{dop} is increased, by 0.15 eV to 5.45 eV at most. This increase in ionization energy is attributed to the fact that a fraction of the α -NPD molecules is positively charged, which makes electron removal energetically more costly. In addition, we have indications for phase separation between F₆TCNNQ-doped α -NPD and pristine F₆TCNNQ at high N_{dop} from x-ray scattering experiments (see SI figure S8). This implies heterogeneity in the local sample work function, which can impact the reliability of the ionization energy determination by PES, as the method is area-averaging [36, 37]. The C1s and the N1s core level peaks shift by up to 0.95 eV towards lower binding energy, indicating a stronger energy level bending in the organic layer with increasing N_{dop} , as expected for a higher density of mobile charge carriers for higher doping concentrations. In addition, the O1s and Zn2p_{3/2} core levels shift by up to 0.50 eV towards lower binding energy due to charge transfer between ZnO and F₆TCNNQ, i.e. a substantial change of surface band bending in the inorganic semiconductor. We note that the morphology of the organic thin film can also influence the electronic properties of the p-n junction. However, SFM and x-ray scattering experiments show that, for moderate doping concentration, the film morphology is similar for different doping concentrations, showing that the morphology does not play a major role in our case (see SI for details).

Conclusion

We investigated the effect of p-doping of the organic semiconductor α -NPD on the energy level alignment at the interface to the inorganic semiconductor ZnO (natively n-type) using photoelectron spectroscopy. When deposited directly on ZnO, F₆TCNNQ is found to chemisorb and reduce the binding energy of the HOMO onset, with respect to the Fermi level, of subsequently deposited α -NPD by 0.95 eV, while simultaneously altering the ZnO surface termination by reducing the OH surface species. For the reverse deposition sequence, and also for the deposition of F₆TCNNQ-doped α -NPD, we find no indication for notable diffusion of the dopant through α -NPD and preferential adsorption on ZnO. Doping α -NPD with 2 vol% F₆TCCNQ induces mobile holes within α -NPD,

but the doping efficiency is low (about 5%). Yet, this enables the formation of a space-charge region within doped α -NPD and concomitant downward energy bending toward the interface to ZnO. Accordingly, the initially downward surface band bending within ZnO is reversed to upward, and the overall features of the interfacial energy levels of this organic/inorganic junction correspond indeed to that of conventional inorganic pn-junctions. With increasing doping concentration, band and energy level bending on both sides of the junction become more pronounced. The detailed understanding of the electronic properties of the prototypical organic/inorganic pn-junction established here facilitates the implementation and optimization of such hybrid heterojunctions in electronic and optoelectronic devices.

Acknowledgments

This work was supported by the SFB951 of Deutsche Forschungsgemeinschaft (DFG).

ORCID iDs

Moritz H Futscher  <https://orcid.org/0000-0001-8451-5009>

Thorsten Schultz  <https://orcid.org/0000-0002-0344-6302>

Norbert Koch  <https://orcid.org/0000-0002-6042-6447>

References

- [1] Lüssem B, Keum C M, Kasemann D, Naab B, Bao Z and Leo K 2016 Doped organic transistors *Chem. Rev.* **116** 13714–51
- [2] Reineke S, Lindner F, Schwartz G, Seidler N, Walzer K, Lüssem B and Leo K 2009 White organic light-emitting diodes with fluorescent tube efficiency *Nature* **459** 234–8
- [3] Meerheim R, Körner C and Leo K 2014 Highly efficient organic multi-junction solar cells with a thiophene based donor material *Appl. Phys. Lett.* **105** 063306
- [4] Sze S M 2014 *Physics of Semiconductor Devices* vol 10 (New York: Wiley)
- [5] Tietze M L, Burtone L, Riede M, Lüssem B and Leo K 2012 Fermi level shift and doping efficiency in p-doped small molecule organic semiconductors: a photoelectron spectroscopy and theoretical study *Phys. Rev. B* **86** 035320
- [6] Salzmänn I and Heimel G 2015 Toward a comprehensive understanding of molecular doping organic semiconductors (review) *J. Electron Spectrosc. Relat. Phenom.* **204** 208–22
- [7] Oehzelt M, Akaike K, Koch N and Heimel G 2015 Computer modeling: energy-level alignment at organic heterointerfaces *Sci. Adv.* **1** e1501127
- [8] Harada K, Werner A G, Pfeiffer M, Bloom C J, Elliott C M and Leo K 2005 Organic homojunction diodes with a high built-in potential: interpretation of the current-voltage characteristics by a generalized einstein relation *Phys. Rev. Lett.* **94** 036601
- [9] Zhang F and Kahn A 2018 Investigation of the high electron affinity molecular dopant F6-TCNNQ for hole-transport materials *Adv. Funct. Mater.* **28** 1703780
- [10] Schlesinger R *et al* 2013 Controlling the work function of ZnO and the energy-level alignment at the interface to organic semiconductors with a molecular electron acceptor *Phys. Rev. B* **87** 155311
- [11] Schultz T *et al* 2016 Tuning the work function of GaN with organic molecular acceptors *Phys. Rev. B* **93** 125309
- [12] Olthof S, Tress W, Meerheim R, Lüssem B and Leo K 2009 Photoelectron spectroscopy study of systematically varied doping concentrations in an organic semiconductor layer using a molecular p-dopant *J. Appl. Phys.* **106** 103711
- [13] Amsalem P, Wilke A, Frisch J, Niederhausen J, Vollmer A, Rieger R, Müllen K, Rabe J P and Koch N 2011 Interlayer molecular diffusion and thermodynamic equilibrium in organic heterostructures on a metal electrode *J. Appl. Phys.* **110** 113709
- [14] Duhm S, Salzmänn I, Bröker B, Glowatzki H, Johnson R L and Koch N 2009 Interdiffusion of molecular acceptors through organic layers to metal substrates mimics doping-related energy level shifts *Appl. Phys. Lett.* **95** 093305
- [15] Gao W and Kahn A 2001 Controlled p-doping of zinc phthalocyanine by coevaporation with tetrafluorotetracyanoquinodimethane: a direct and inverse photoemission study *Appl. Phys. Lett.* **79** 4040–2
- [16] Timpel M, Li H, Nardi M V, Wegner B, Frisch J, Hotchkiss P J, Marder S R, Barlow S, Brédas J L and Koch N 2018 Electrode work function engineering with phosphonic acid monolayers and molecular acceptors: charge redistribution mechanisms *Adv. Funct. Mater.* **28** 1704438
- [17] Greiner M T, Helander M G, Tang W M, Wang Z B, Qiu J and Lu Z H 2012 Universal energy-level alignment of molecules on metal oxides *Nat. Mater.* **11** 76–81
- [18] Yang J P, Li Y Q, Duhm S, Tang J X, Kera S and Ueno N 2014 Molecular structure-dependent charge injection and doping efficiencies of organic semiconductors: impact of side chain substitution *Adv. Mater. Interfaces* **1** 1300128
- [19] Gao W and Kahn A 2003 Controlled p doping of the hole-transport molecular material N,N'-diphenyl-N,N'-bis(1-naphthyl)-1,1'-biphenyl-4,4'-di amine with tetrafluorotetracyanoquinodimethane *J. Appl. Phys.* **94** 359–66
- [20] Hill I G and Kahn A 1998 Energy level alignment at interfaces of organic semiconductor heterostructures *J. Appl. Phys.* **84** 5583–6
- [21] Rangger G M, Hofmann O T, Romaner L, Heimel G, Bröker B, Blum R P, Johnson R L, Koch N and Zojer E 2009 F4TCNQ on Cu, Ag, and Au as prototypical example for a strong organic acceptor on coinage metals *Phys. Rev. B* **79** 165306
- [22] Amsalem P, Niederhausen J, Frisch J, Wilke A, Bröker B, Vollmer A, Rieger R, Müllen K, Rabe J P and Koch N 2011 Metal-to-acceptor charge transfer through a molecular spacer layer *J. Phys. Chem. C* **115** 17503–7
- [23] Kleemann H, Schuenemann C, Zakhidov A A, Riede M, Lüssem B and Leo K 2012 Structural phase transition in pentacene caused by molecular doping and its effect on charge carrier mobility *Org. Electron.* **13** 58–65
- [24] Méndez H *et al* 2015 Charge-transfer crystallites as molecular electrical dopants *Nat. Commun.* **6** 8560
- [25] Li H, Schirra L K, Shim J, Cheun H, Kippelen B, Monti O L A and Brédas J L 2012 Zinc oxide as a model transparent conducting oxide: a theoretical and experimental study of the impact of hydroxylation, vacancies, interstitials, and extrinsic doping on the electronic properties of the polar ZnO (0002) surface *Chem. Mater.* **24** 3044–55
- [26] Blochwitz J, Fritz T, Pfeiffer M, Leo K, Alloway D M, Lee P A and Armstrong N R 2001 Interface electronic structure of organic semiconductors with controlled doping levels *Org. Electron.* **2** 97–104
- [27] Colinge J-P and Colinge C A 2002 *Physics of Semiconductor Devices* (Dordrecht: Kluwer)

- [28] Hamwi S, Meyer J, Winkler T, Riedl T and Kowalsky W 2009 p-type doping efficiency of MoO₃ in organic hole transport materials *Appl. Phys. Lett.* **94** 253307
- [29] Lüssem B, Riede M and Leo K 2013 Doping of organic semiconductors *Phys. Status Solidi* **210** 9–43
- [30] Kröger M, Hamwi S, Meyer J, Riedl T, Kowalsky W and Kahn A 2009 P-type doping of organic wide band gap materials by transition metal oxides: a case-study on Molybdenum trioxide *Org. Electron.* **10** 932–8
- [31] Pingel P and Neher D 2013 Comprehensive picture of p-type doping of P3HT with the molecular acceptor F4TCNQ *Phys. Rev. B* **87** 115209
- [32] Pingel P, Zhu L, Park K S, Vogel J O, Janietz S, Kim E G, Rabe J P, Brédas J L and Koch N 2010 Charge-transfer localization in molecularly doped thiophene-based donor polymers *J. Phys. Chem. Lett.* **1** 2037–41
- [33] Tietze M L, Benduhn J, Pahner P, Nell B, Schwarze M, Kleemann H, Krammer M, Zojer K, Vandewal K and Leo K 2018 Elementary steps in electrical doping of organic semiconductors *Nat. Commun.* **9** 1182
- [34] Tietze M L, Leo K and Lüssem B 2013 Quantification of deep hole-trap filling by molecular p-doping: dependence on the host material purity *Org. Electron.* **14** 2348–52
- [35] Ghani F, Opitz A, Pingel P, Heime G, Salzmänn I, Frisch J, Neher D, Tsami A, Scherf U and Koch N 2015 Charge transfer in and conductivity of molecularly doped thiophene-based copolymers *J. Polym. Sci. B* **53** 58–63
- [36] Schultz T, Lenz T, Kotadiya N, Heime G, Glasser G, Berger R, Blom P W M, Amsalem P, de Leeuw D M and Koch N 2017 Reliable work function determination of multicomponent surfaces and interfaces: the role of electrostatic potentials in ultraviolet photoelectron spectroscopy *Adv. Mater. Interfaces* **4** 1700324
- [37] Schultz T, Amsalem P, Kotadiya N B, Lenz T, Blom P W M and Koch N 2018 Importance of substrate work function homogeneity for reliable ionization energy determination by photoelectron spectroscopy *Phys. Status Solidi* accepted (<https://doi.org/10.1002/pssb.201800299>)